

Next-generation test of cosmic inflation

Benjamin Gold* and Andreas Albrecht

Department of Physics, UC Davis, One Shields Avenue, Davis CA, USA 95616

(Dated: January 3, 2003)

The increasing precision of cosmological datasets is opening up new opportunities to test predictions from cosmic inflation. Here we study the impact of high precision constraints on the primordial power spectrum and show how a new generation of observations can provide impressive new tests of the slow-roll inflation paradigm, as well as producing significant discriminating power among different slow-roll models. In particular, we consider next-generation measurements of the Cosmic Microwave Background (CMB) temperature anisotropies and (especially) polarization, as well as new Lyman- α measurements that could become practical in the near future. We emphasize relationships between the slope of the power spectrum and its first derivative that are nearly universal among existing slow-roll inflationary models, and show how these relationships can be tested on several scales with new observations. Among other things, our results give additional motivation for an all-out effort to measure CMB polarization.

PACS numbers: 98.80.Cq

I. INTRODUCTION

Over the last several years, extraordinary observational support has emerged for the idea that key features of our universe were formed by a period of cosmic inflation. During inflation, the universe enters a period of “superluminal expansion” which imprints certain features on the universe. The physical degree of freedom responsible for inflation, generically called the “inflaton”, has yet to find a comfortable home in fundamental theory, and there are many competing ideas for how fundamental aspects of inflation could play out. None the less, at the phenomenological level a standard picture of inflation has emerged.

From the observational point of view, the standard picture is defined by a set of observable characteristics that are the same across virtually all proposed models for the inflaton. The most well known predictions from the standard picture of inflation are that the universe has critical density (to within roughly one part in 10^5), that the primordial perturbations are coherent, (leading, for example, to acoustic peaks in the microwave background power spectrum), and that the power spectrum of primordial perturbations is nearly scale invariant, with the tilt parameter n_s constrained to be close to unity. A unique spectrum of coherent gravitational waves is also predicted, which could eventually come within range of direct gravitational wave detectors, and which could also be observed indirectly via signals in the microwave background polarization.

But inflation makes many more predictions than these. Specifically, a given model for the inflaton will predict a detailed shape for the primordial power spectrum that goes way beyond what can be described simply by a single tilt parameter. The detailed shape of the power

spectrum is a reflection of the particular evolution of the inflaton during inflation, something that is precisely specified in a given model. In this paper we show how the next generation of experiments could bring studies of the power spectrum shape to a whole new level. These studies present two kinds of opportunities: One opportunity is to make additional tests of the standard picture of inflation. To this end, we focus on particular power spectrum features that are known to exist across essentially all inflation models. The search for these features could either confirm or falsify the standard picture of inflation.

The second opportunity is to go beyond broad tests of the standard picture. The next generation of experiments which we consider here will provide important additional information. This information could actually distinguish among different specific inflaton models, assuming the standard model is not falsified, or it could provide very useful constraints on the alternatives if the standard model is ruled out.

Our approach here is similar to and inspired by a large body of earlier work on this subject [1, 2, 3, 4, 5, 6, 7, 8, 9]. Our emphasis here is identifying what useful information about the primordial power spectrum and inflation might be revealed by a new generation of experiments. For this work we assume that the primordial perturbations are adiabatic. As emphasized in [10], relaxing this assumption would result in more degeneracies and would lead to somewhat weaker constraints on parameters.

The organization of this paper is as follows: Section II gives background information about slow roll inflation. Section II A introduces the aspects of slow roll inflation we intend to test. Section III discusses the CMB and Lyman- α data (existing and simulated) we use to test inflation. Section IV gives our main results and V gives our conclusions. Appendix A gives details of the inflation models we use for our plots and appendix B gives more detailed results.

*Electronic address: gold@bubba.ucdavis.edu

II. SCALAR FIELD INFLATION

In the standard picture, inflation occurs when the potential energy density $V(\phi)$ of a scalar field ϕ (the inflaton) dominates the stress-energy [11, 12, 13, 14]. This scalar field may be a true scalar field or an effective field obtained from some more complicated theory. The period of potential domination is usually closely connected to very slow evolution of the inflaton field, the so-called “slow roll” behavior, and it is this slow evolution that produces a nearly scale invariant spectrum of perturbations. In the slow roll inflationary scenario, however, ϕ , and therefore $V(\phi)$, are not completely constant during inflation, and this leads to deviations from total scale invariance.

The dynamic behavior of the potential is determined by the equation of motion for a scalar field in an expanding universe

$$\ddot{\phi} + 3H\dot{\phi} + V'(\phi) = 0. \quad (1)$$

The gradient of the field is ignored, as even if present it will be quickly damped by the inflationary expansion to the degree that it is irrelevant for the evolution of the background spacetime, which is what we determine from Eqn. 1. The field is considered to be in a slow roll regime if $\dot{\phi}$ is negligible. The Hubble constant $H \equiv \dot{a}/a$ is related to the total energy density of the universe which if dominated by the scalar field is

$$H^2 = \frac{1}{3} \left(\frac{1}{2} \dot{\phi}^2 + V(\phi) \right), \quad (2)$$

where $M_P \equiv 1/\sqrt{8\pi G}$ has been set to unity. It is customary to define slow roll parameters such as

$$\epsilon \equiv \frac{1}{2} \left(\frac{V'}{V} \right)^2, \quad \eta \equiv \frac{V''}{V}, \quad \xi^2 \equiv \frac{V'V'''}{V^2}, \quad (3)$$

although several other conventions also exist in the literature. Assuming that these parameters (and the higher derivatives of V) are small leads to expressions for the primordial amplitude of density perturbations [15]

$$|A_S(k)| = \frac{\delta\rho}{\rho} = \frac{H}{\sqrt{2}\epsilon}, \quad (4)$$

the spectral index of these perturbations

$$n_S(k) \equiv \frac{d \ln k A_S^2(k)}{d \ln k} = 1 + 2\eta - 6\epsilon, \quad (5)$$

and the derivative of the spectral index

$$n_S'(k) \equiv \frac{dn_S(k)}{d \ln k} = -2\xi^2 + 16\eta\epsilon - 24\epsilon^2. \quad (6)$$

The right-hand side of each equation above is to be evaluated during inflation at the time when the scale of interest k exits the Hubble radius.

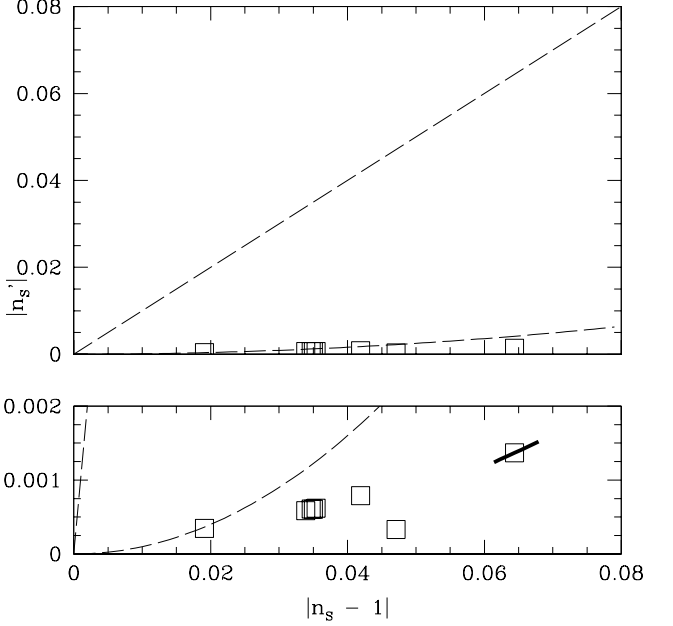


FIG. 1: The values of n_S and n_S' at CMB scales are plotted for several models. The lower graph is a zoomed view of the bottom of the upper graph. In both, the upper line is $n_S' = n_S - 1$ and the lower line is $n_S' = (n_S - 1)^2$. The thick line on the lower graph shows the evolution of n_S and n_S' with scale for two orders of magnitude in each direction.

A. Slow roll, n_S , and n_S'

A general feature of slow roll is that n_S' is higher order in the slow roll parameters than n_S . Thus if we assume higher order terms become increasingly small, then barring a conspiracy of cancellation between terms $|n_S'| \sim (n_S - 1)^2$ or less. As pointed out in [16], while this assumption is commonly made it is technically an addition to the common assumption that the slow roll parameters are small. We emphasize that while detection of a large n_S' would not completely rule out slow roll, it would force a rethinking of the standard picture of inflation. This relation can be generalized to higher derivatives, resulting in a kind of consistency relation

$$\left| \frac{d^n n_S}{d \ln k^n} \right| \leq |n_S - 1|^{n+1}. \quad (7)$$

For inflationary scenarios involving multiple fields (often called hybrid models) this condition is relaxed. With multiple fields the extra freedom introduced makes it easier to remain on the edge of violating the slow roll conditions over many e-foldings. Thus the tendency for models to lie under the curve $|n_S'| = (n_S - 1)^2$ is not as strong for hybrid models.

To discuss observational constraints, we take the point of view of [17] that the primordial power spectrum is an unknown function, which may be sampled by experiments at one or more scales. Statements about the slope

of this function (and higher derivatives) then can only be tested by effectively sampling the function to high accuracy at several nearby scales. Current analysis tends to use all the data to provide only limited information about the power spectrum. We wish to emphasize that higher quality data over a range of scales will allow us extract significantly more information about the primordial power spectrum, information that can have a great impact on tests of the inflationary picture.

B. Model space

One of the simplest models to evaluate is a pure exponential. For $V = V_0 \exp(\lambda\phi)$ the spectral index $n_S = 1 - \lambda^2$ for all scales, and thus n_S' and all higher derivatives are zero. Thus for this model measurements of n_S simply map into constraints on λ , without presenting an opportunity to falsify the general model. But a measurement of n_S' which excludes zero can rule this type of inflaton potential altogether.

This model is special in that the potential is constructed to form the simplest possible power law spectrum of perturbations. Most inflationary models have more complicated forms, but many proposed models approximate the exponential behavior on the scales which cosmological measurements probe. An example of a very different kind of potential is given by Stewart and Lyth[16]. This potential has been constructed to have $|n_S'| \sim |n_S - 1|$ over a range of scales, and results in a markedly different primordial power spectrum.

A previous survey of models of inflation and their spectral index can be found in [18]. In figure 1 several different models taken from a sampling of the literature have been plotted. (Specific information about each model plotted is given in appendix A.) The types of models range from high-order polynomial to mass-term to brane-world inspired scenarios [14, 19, 20, 21, 22]. Despite the difference in the form of each model's potential, all of them live on or below the line $|n_S'| = (n_S - 1)^2$.

III. DETERMINING HOW WELL EXPERIMENTS CAN DO

To find the possible impact of CMB and Lyman- α experiments, we model the primordial power spectrum with a Taylor series expansion of the spectral index around a particular scale

$$A_S^2(k) = P \left(\frac{k}{k^*} \right)^{-1+n_S+n_S'x+\frac{1}{2}n_S''x^2+\dots}, \quad (8)$$

where $x \equiv \ln(k/k^*)$, k^* is the pivot point, and P is an overall normalization. We then use Fisher matrix techniques to jointly estimate parameters for each experiment.

Parameterizing the power spectrum a particular way has its own set of advantages and disadvantages. One

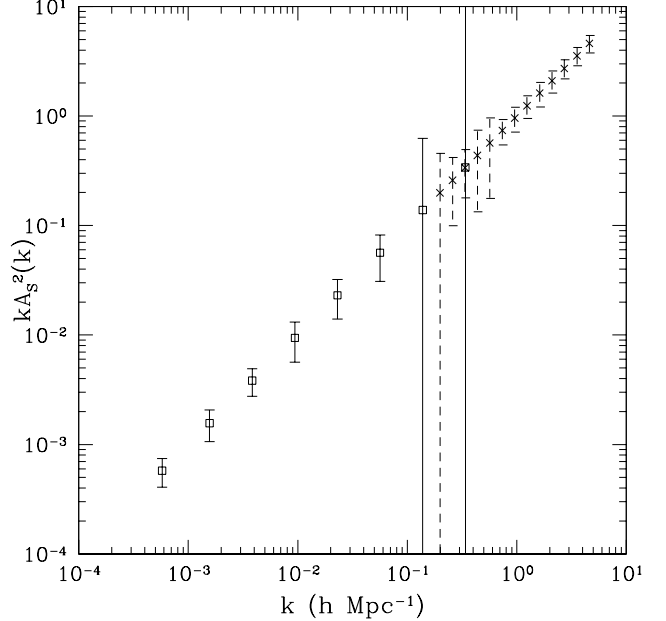


FIG. 2: One-sigma error in the primordial power spectrum from a MAP-like microwave anisotropy temperature and polarization experiment (squares with solid error bars), and from a Lyman- α experiment as in [23] (crosses with dashed error bars).

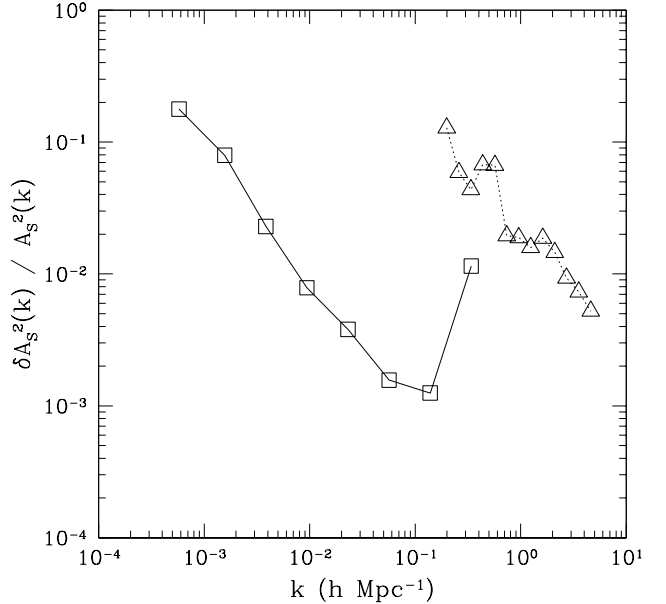


FIG. 3: One-sigma error in the primordial power spectrum from an after-Planck temperature and polarization experiment (squares), and from a Lyman- α experiment with statistical uncertainties one hundred times smaller than current experiments (triangles).

nice feature of the step-wise form of [24] is that it is easy for each bin amplitude to be a nearly statistically independent parameter in the likelihood analysis. The coefficients of a Taylor series expansion generally have larger covariances. The disadvantage of the step-wise form, however, is that the quantities of interest to us (such as the spectral index) are not simply related to the shape parameters.

A. CMB

We first consider CMB experiments which measure both the temperature and polarization anisotropies. For scalar perturbations there are three power spectra described by $C_\ell^{(T,E,C)}$, where (T, E, C) indicate the temperature, E -mode polarization, and cross-correlation power spectra. These C_ℓ all have similar dependence on the primordial power spectrum, and are found by

$$C_\ell = (4\pi^2) \int \frac{dk}{k} A_S^2(k) |\Delta_\ell(k, \tau = \tau_0)|^2, \quad (9)$$

where $\Delta_\ell(k, \tau = \tau_0)$ are transfer functions for the CMB, and $A_S^2(k)$ is the squared amplitude of the primordial power spectrum. The functions $\Delta_\ell(k, \tau = \tau_0)$ depend on cosmological parameters, and can be conveniently calculated using the CMBFAST code [25].

Error in a cosmological parameter s_i can be estimated as $\sqrt{(\mathbf{F}^{-1})_{ii}}$, where \mathbf{F} is the Fisher matrix

$$F_{ij} = \sum_{I,J=(T,E,C)} \sum_\ell \frac{\partial C_\ell^I}{\partial s_i} (\mathbf{C}^{-1})_{IJ} \frac{\partial C_\ell^J}{\partial s_j}. \quad (10)$$

The covariance matrix \mathbf{C} has elements which can be approximated by [2]

$$C_{TT} = \frac{2}{(2\ell+1)f_{\text{sky}}} (C_\ell^T + N_\ell^T)^2, \quad (11)$$

$$C_{EE} = \frac{2}{(2\ell+1)f_{\text{sky}}} (C_\ell^E + N_\ell^E)^2, \quad (12)$$

$$C_{CC} = \frac{1}{(2\ell+1)f_{\text{sky}}} \times [(C_\ell^C)^2 + (C_\ell^T + N_\ell^T)(C_\ell^E + N_\ell^E)], \quad (13)$$

for the diagonal elements, and the off-diagonal elements are

$$C_{TE} = \frac{2}{(2\ell+1)f_{\text{sky}}} (C_\ell^C)^2, \quad (14)$$

$$C_{TC} = \frac{2}{(2\ell+1)f_{\text{sky}}} C_\ell^C (C_\ell^T + N_\ell^T), \quad (15)$$

$$C_{EC} = \frac{2}{(2\ell+1)f_{\text{sky}}} C_\ell^C (C_\ell^E + N_\ell^E). \quad (16)$$

In equations 11 through 16, f_{sky} is the fractional sky coverage of the experiment, and we have defined a noise

term

$$N_\ell^{(T,E)} \equiv \sigma_{(T,E)}^2 \theta_{\text{fwhm}}^2 e^{(0.425 \theta_{\text{fwhm}} \ell)^2}, \quad (17)$$

where $\sigma_{(T,E)}$ is the noise per pixel in the temperature and polarization measurements and θ_{fwhm} is the width of the beam. For experiments like MAP which obtain temperature and polarization data by adding and differencing two polarization states, the noise per pixel for each is related by $\sigma_T^2 = \sigma_E^2/2$.

The derivatives $\partial C_\ell / \partial s_i$ are evaluated via finite difference using a numerical code derived from CMBFAST and DASH [26]. We consider only flat models, using as parameters $\Omega_b h^2$, $\Omega_m h^2$, Ω_Λ , $\exp(-2\tau)$, the primordial power spectrum normalization P , and the first seven coefficients in the expansion of n_S . The Fisher matrix calculation for the errors in the parameters also assumes a “true” model around which the derivatives are taken; for this we use a Λ CDM model with $\Omega_b h^2 = 0.015$, $\Omega_m h^2 = 0.0862$, $\Omega_\Lambda = 0.7$, $\tau = 0$, and a flat primordial power spectrum.

B. Lyman- α

For the Lyman- α data, the error bars that were reported in [23] for the linear matter power spectrum are used. The primordial power spectrum is related to the linear matter power spectrum by

$$P_{\text{LM}}(k) = P_0 k A_S^2(k) T^2(k), \quad (18)$$

where $T^2(k)$ is the transfer function and contains the dependence upon cosmological parameters, and P_0 is a normalizing constant. Then the error bars for the power spectrum parameters are calculated via standard error propagation techniques using the previous equation and the analytic form for the transfer function [27]

$$T(q) = \frac{\ln(1 + 2.34q)}{2.34q} \times [1 + aq + (bq)^2 + (cq)^3 + (dq)^4]^{-\frac{1}{4}}, \quad (19)$$

where $q \equiv k/\Omega h^2 \exp(-2\Omega_b)$ and a, b, c, d are fit parameters which are irrelevant to the error analysis. We use the results of the CMB parameter estimation as inputs for determining the errors in h , Ω , and Ω_b .

The large systematic normalization error reported in [23] is a problem for estimating primordial power spectrum amplitudes, but does not affect local estimates of the slope or higher derivatives, so we do not include it.

C. Error contours for current and future data

An illustration of CMB and Lyman- α constraints on the primordial power spectrum are shown in figures 2 and 3. If we fit a function to all the data points, and assume that function to be linear then of course the slope will be

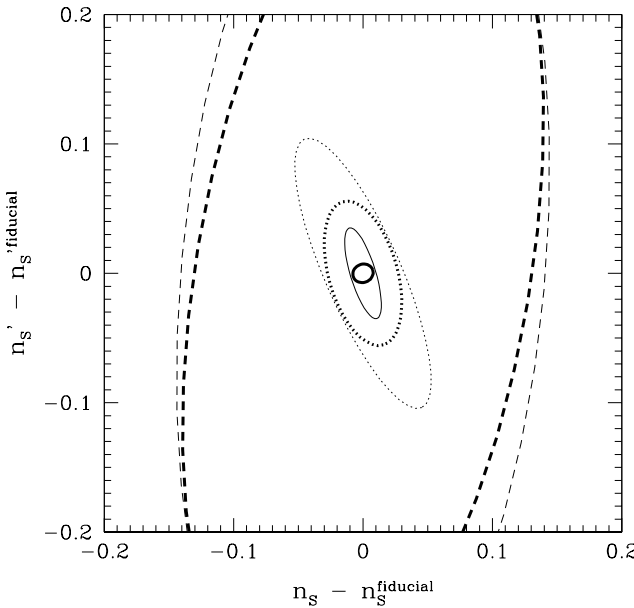


FIG. 4: 68% confidence regions in the $n_s - n_s'$ plane for various experiments of the sort described in table I. The MAP-like constraints are shown dashed, PLANCK-like dotted, and Next-Generation constraints solid. We use prior I-6 as described in section IV. Constraints with(without) polarization are drawn with thick(thin) lines.

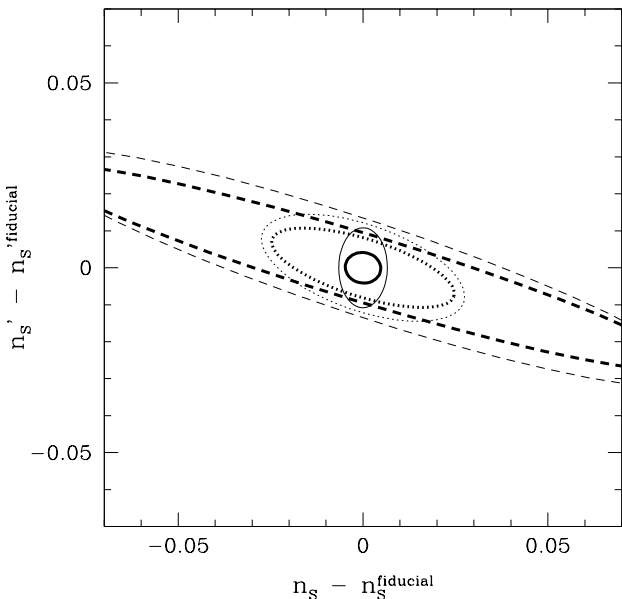


FIG. 5: 68% confidence regions in the $n_s - n_s'$ plane for the same experiments as in figure 4, only now using prior IIb as described in section IV. Note: The window of this plot is greatly “zoomed in” compared with figure 4.

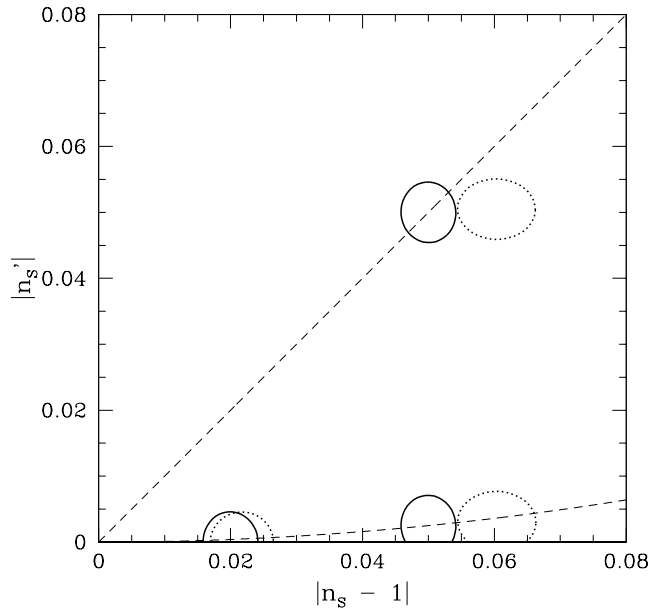


FIG. 6: Solid contours show constraints in the $n_s - n_s'$ plane from the CMB data of the “super” experiment of table I (using prior I-6) for scales near $k = 0.0565$. Several different fiducial models are shown, two representative of the types shown in figure 1 and one large- n_s' model of the type described in [16]. The dotted contours are the result of assuming the consistency relation of equation 7 and extrapolating from CMB scales to Lyman- α scales ($k = 2.39$). If the relation is valid, constraints from the two types of data will be correlated in this plane as illustrated by the pairs of adjacent solid and dashed contours. All contours are drawn enclosing regions of 68% confidence level.

TABLE I: Noise parameters used for simulating various experiments.

Experiment	σ_T	θ_{fwhm}	f_{sky}
MAP-like	$27 \mu\text{K}$	$12.6'$	0.7
PLANCK-like	$10 \mu\text{K}$	$9'$	0.7
Next-Generation	$2.7 \mu\text{K}$	$4.8'$	0.7
Super	$0.27 \mu\text{K}$	$1.8'$	0.7

tightly constrained. If we allow the function to have a more complicated shape, the slope at any point becomes less well constrained. Figure 2 roughly represents current experimental limits. The main point of this paper is that future data can become good enough to loosen the assumptions on the shape and still produce very tight constraints. This is shown in figure 3, which represents some future experiments accurate enough to clearly distinguish a model with $n_s' = 0.05$ from a model with $n_s' = (0.05)^2$, even using data spanning only one order of magnitude in wavenumber.

The ultimate limiting factor in how precise all these measurements can be is due to cosmic variance. For the

TABLE II: Marginalized errors ($\times 1000$) in n_S and n_S' for simulated experiments with different priors on truncating the Taylor expansion of the spectral index. Power spectrum parameters are amplitude, tilt (n_S), and for column I- m , the first m derivatives of the tilt.

Experiment	prior I-6 $\delta n_S, \delta n_S'$ ($\times 1000$)	prior I-3 $\delta n_S, \delta n_S'$ ($\times 1000$)	prior I-1 $\delta n_S, \delta n_S'$ ($\times 1000$)
MAP-like w polarization	96.3, 258	86.0, 56.6	58.1, 19.5
	93.3, 229	81.9, 47.4	55.6, 16.2
PLANCK-like w polarization	35.2, 69.8	21.0, 27.6	18.4, 8.86
	20.0, 37.3	17.5, 19.9	16.5, 5.76
Next-Gen w polarization	9.46, 23.4	8.00, 16.1	4.27, 6.21
	5.24, 4.79	4.35, 3.24	2.90, 2.28
Super w polarization	7.12, 16.6	6.20, 13.3	3.38, 5.08
	2.78, 3.07	2.36, 1.68	1.51, 1.29

CMB, the fractional error from this effect is $\Delta C_\ell/C_\ell \sim 1/\sqrt{\ell}$, which means even for large ℓ each individual C_ℓ can only ever be known to within a few percent.

From figure 3 we can see that the CMB accurately probes the primordial power spectrum at somewhat larger scales than those where the Lyman- α data is most accurate. This means the two experiments provide constraints on n_S and n_S' at different scales, allowing us to further test our models by looking at how they predict these quantities should change with wavenumber. We will explore this idea further in section IV.

To then make error contours in the n_S - n_S' plane, we use the covariance matrix from the parameter analysis to marginalize over other parameters and determine the covariance matrix for just n_S and n_S' . Of the four hypothetical CMB experiments listed in table I, we show how well the first three place constraints in the n_S - n_S' plane (for two different priors) in figures 4 and 5. We examine the fourth experiment (the best) in detail (using the weakest prior) in figure 6. These results are discussed at length in the following section. For hypothetical Lyman- α experiments, we do not understand the physics connecting the primordial power spectrum to measurements as well as for the CMB. We therefore “simulate” improvements in experiments as an overall reduction in statistical uncertainty due to larger samples, and an improved knowledge of the transfer function due to decreased errors in h , Ω , and Ω_b .

IV. TESTING INFLATION

A. Results

For completeness, we discuss a range of possible priors, each of which represents a different points of view on what one wants to take as an assumption and what one is trying to test. In tables II and III we report the

TABLE III: Marginalized errors ($\times 1000$) in n_S and n_S' for simulated experiments with different priors on the higher derivatives of the spectral index. Prior I-6 from Table II above is for reference. Priors IIa and IIb use all six derivatives in the joint parameter estimation, but IIa imposes the constraint that all higher (n_S'' and above) derivatives are within 0.01 of scale invariant, and IIb imposes the consistency relation (Eqn. 7) on the higher derivatives.

Experiment	prior I-6 $\delta n_S, \delta n_S'$ ($\times 1000$)	prior IIa $\delta n_S, \delta n_S'$ ($\times 1000$)	prior IIb $\delta n_S, \delta n_S'$ ($\times 1000$)
MAP-like w polarization	96.3, 258	80.2, 28.7	60.3, 21.5
	93.3, 229	77.5, 26.5	57.8, 18.5
PLANCK-like w polarization	35.2, 69.8	18.7, 10.4	18.4, 9.86
	20.0, 37.3	16.9, 8.31	16.5, 7.17
Next-Gen w polarization	9.46, 23.4	4.59, 8.09	4.40, 7.23
	5.24, 4.79	3.41, 3.07	3.21, 2.77
Super w polarization	7.12, 16.6	3.69, 6.97	3.52, 6.20
	2.78, 3.07	2.08, 1.79	1.93, 1.48

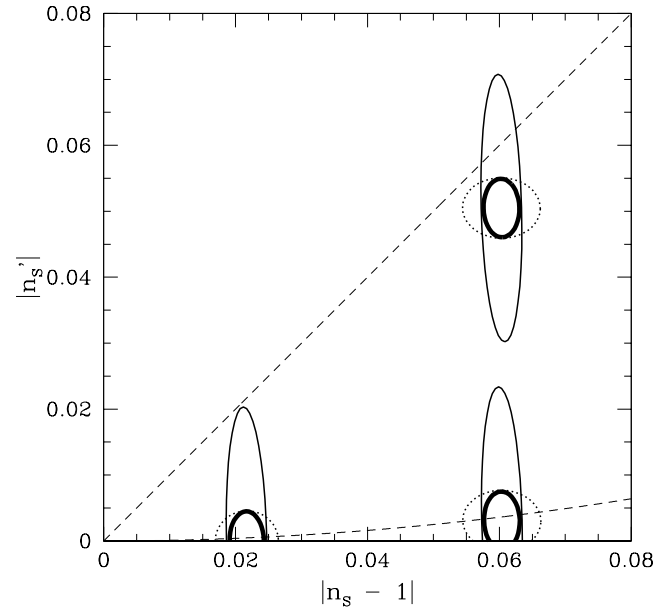


FIG. 7: Constraints in the n_S - n_S' plane from the Lyman- α data of figure 3 for scales near $k = 2.39$ (thin large ovals). The projected ovals from figure 6 (dotted ovals) are then combined with the Lyman- α data to form improved constraints (thick small ovals). Again, 68% confidence level regions are plotted.

constraints that various CMB experiments can place on n_S and n_S' . Our weakest prior, which we refer to as I-6, is simply to use the four cosmological parameters ($\Omega_b h^2, \Omega_m h^2, \Omega_\Lambda, \tau$) and eight power spectrum parameters (P and the first seven coefficients in the expansion of n_S). Having so many parameters for the power spectrum allows the shape to vary quite a bit, and loosens

constraints on each term of the expansion.

To get better constraints requires either using a more restrictive prior or improving the experiment. In table II we change the prior by using fewer power spectrum parameters. Prior I-3 uses only the first four terms of the expansion of n_S (i.e. up to third order), and prior I-1 uses only the first two terms, such that the only power spectrum parameters for prior I-1 are amplitude, n_S , and n_S' . In table III we change the prior by placing a priori constraints on the higher derivative terms of the expansion, rather than dropping them completely. Prior IIa supposes that all the higher derivative terms (n_S'' and higher) are “small”, less than 0.01. Prior IIb also imposes the constraint that the higher derivatives be “small”, but supposes they fall off in the form of the consistency relation of equation 7.

Prior I-6 represents the weakest assumptions, and prior I-1 the tightest assumptions. (Prior I-1 basically adds just one new parameter, n_S' , to the canonical set.) Prior IIb represents an assumption of the standard inflationary picture for the higher derivatives, but places no prior constraint in the $n_S - n_S'$ plane so it those parameters can be used to test the standard picture. (Of course, if the standard slow roll picture fails, prior IIb may no longer be of interest)

We have simulated CMB experiments with and without polarization measurements. Since the primordial power spectrum affects the CMB temperature and polarization in exactly the same way, naively polarization simply adds a second way of measuring the same thing and should only reduce uncertainty by a factor of $\sqrt{2}$. However, allowing joint estimation of other cosmological parameters in addition to those describing the shape of the primordial power spectrum introduces confusion and near-degeneracies. The value of measuring polarization is not so much that it directly puts limits on the power spectrum, but in reducing the confusion with other parameters. Our analysis shows the increasing value of polarization as CMB experiments get better and better. Furthermore, they show that better experiments will also be able to provide constraints on the primordial power spectrum in a much more prior-independent way than is possible currently. Constraints on all the power spectrum parameters are listed in appendix B.

In figures 6 and 7 we see the error contours in the $n_S - n_S'$ plane for a hypothetical super-Planck CMB temperature and polarization experiment and for a “super” Ly- α survey. We see that such data would provide very significant constraints in this space. In particular, these experiments are good enough to clearly distinguish points on the line $n_S' = n_S - 1$ from the line $n_S' = (n_S - 1)^2$ for all but very small values of n_S , and thus would offer significant tests of the standard inflationary picture.

Combining data from both experiments will provide additional constraints and tests. Each experiment provides constraints in the $n_S - n_S'$ plane, but on somewhat different scales. These amount to providing constraints on the inflaton potential $V(\phi)$ near a particu-

lar wavenumber k . There are several possible options for combining data from several experiments. One approach is to use a single parametrization for the primordial power spectrum and then to jointly estimate all parameters using the full dataset. If both experiments were at the same scale, this would amount to simply overlapping their individual error contours. To perform joint estimation for experiments at different scales, we would want to find parameters that are “good” across different scales. More important for our immediate analysis, however, is that different experiments often have a (sometimes poorly characterized) systematic error in their relative normalization which causes problems for a joint parameter analysis.

For simplicity, then, we choose a second option, which is to look at the two experiments separately and then use the consistency equation (Eqn. 7) to produce the inequality

$$\frac{n_S(k_{\text{Ly}\alpha}) - n_S(k_{\text{CMB}})}{\ln k_{\text{Ly}\alpha} - \ln k_{\text{CMB}}} < (n_S(k_{\text{Ly}\alpha}) - 1)^2 \quad (20)$$

as an additional inflationary test. By looking at only derivatives of the power spectrum we avoid the relative normalization problems. Visually, this amounts to projecting the CMB contours for n_S and n_S' up to Lyman- α scales (or vice-versa) and checking to see if the contours overlap, as shown in figure 7. This third test is not redundant because we use different pivot points ($k_{\text{Ly}\alpha}$ and k_{CMB}) for the different datasets. A potential with large higher derivatives could pass the $n_S' < (n_S - 1)^2$ test at a particular scale and yet fail it when data from different scales is used.

Finally, we would like to remind the reader that for figures 6 and 7, the real information is in the size of the error contours rather than their actual placement. In the absence of real data, we show contours from simulated data for a small sample of models all of which show correlations between the two experiments consistent with the standard inflationary picture. Ultimately nature will tell us if such correlations are really there.

B. Projected errors and cross-correlations

To further show the value of better experiments, we have investigated how the projected errors in n_S and n_S' should change as a result of improving both resolution and noise levels. Figure 8 shows the marginalized errors (with prior I-6) with and without polarization, as functions of beam width and pixel noise.

A source of worry is possible cross-correlation between our power spectrum parameters and other cosmological parameters. Confusion between tilt and optical depth is well-known, and polarization helps greatly at reducing such confusion (see figure 9). However, we found that there is generally a large correlation between Ω_Λ and our power spectrum parameters (of which n_S' is of the most interest), which is only removed by the best experiments

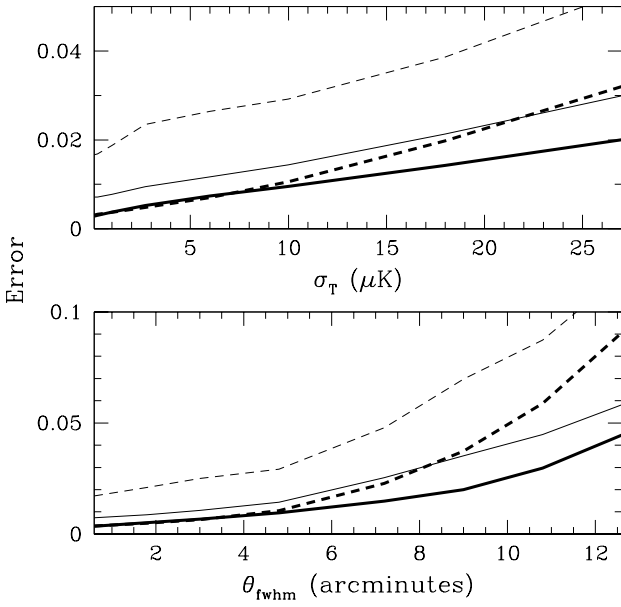


FIG. 8: Marginalized (one-sigma) errors of n_S (solid line) and n_S' (dashed line) as a function of pixel noise and beam width. Values with (without) polarization are shown as thick (thin) lines. For the upper plot, beam width has been fixed at $4.8'$, and for the lower noise has been fixed at $10\mu\text{K}$.

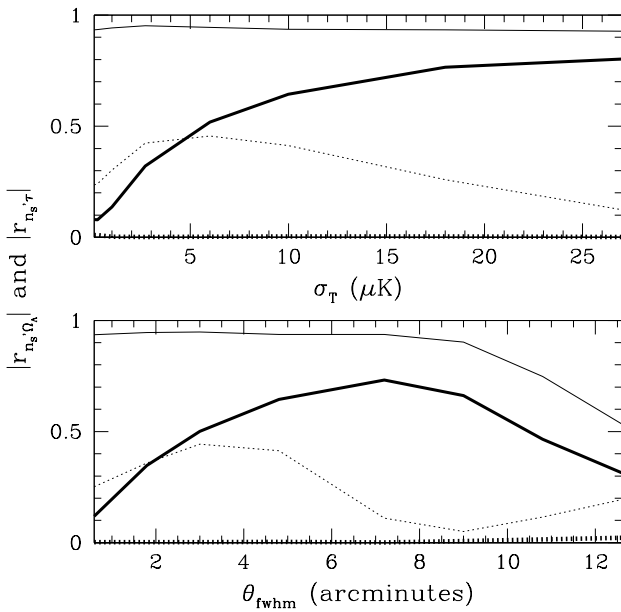


FIG. 9: Cross-correlation between n_S' and Ω_Λ , both with (thick line) and without (thin line) polarization. Cross-correlation between n_S' and τ is shown as the (thick and thin) dotted lines.

with polarization measurements. This suggests that independent determination of Ω_Λ in the near future may be valuable for placing future constraints on inflationary parameters.

V. CONCLUSION

We have shown that the next generation of cosmological experiments should determine the shape of the primordial power spectrum sufficiently to allow new tests of the standard picture of inflation. If the standard picture is upheld, a new level of differentiation among different inflaton potentials will be possible. We have investigated the potential impact of new data on both the CMB and the Lyman- α forest.

The Lyman- α data offers a promising route to testing slow-roll models both on its own, and in conjunction with CMB data. Currently published data does not get too far with this enterprise, but next-generation observation could have considerable impact[29].

For the CMB data, if we are interested in general constraints without placing restrictive priors on the primordial power spectrum, Planck-like CMB experiments do not quite have the precision to put the strong limits on n_S' that we desire. It is not until relatively high ℓ that the uncertainty from cosmological variance is low enough for our requirements, and it is precisely at these high ℓ that the Planck experiment noise rapidly becomes dominant so a further improvement beyond Planck is needed. Our hypothetical “next-generation” experiment should start placing interesting constraints in the n_S – n_S' plane, the “super” experiment does even better. Also important is the measurement of the (E-mode) polarization channel, which is vital to reducing degeneracies that make the tests more challenging.

For constraints on the power spectrum itself (as opposed to other cosmological parameters), information from low multipole moments ($\ell < 200$) contributes very little due to cosmic variance, however these are needed for the full parameter estimation and simply to beat down noise further, so coverage of a large fraction of the sky is needed. Higher multipole moments are useful up until Silk damping reduces the overall CMB signal. As CMB experiments improve, polarization will become even more important as the key to breaking degeneracies between the effects of the power spectrum shape and other cosmological parameters.

Acknowledgments

We thank Lloyd Knox and Manoj Kaplinghat for helpful conversations. We were supported in part by DOE grant DE-FG03-91ER40674.

APPENDIX A: MODELS

The potentials used in the models shown in figure 1, from left to right are (in units where $M_P \equiv 1$)

$$M^4 [1 + A \ln \phi], \quad (A1)$$

$$M^4 \left[1 - e^{-\phi/2} \right]^2, \quad (A2)$$

$$M^4 [1 - e^{-\phi}], \quad (A3)$$

$$M^4 [1 + A\phi^2], \quad (A4)$$

$$M^4 \cos^2 \frac{\phi}{A}, \quad (A5)$$

$$M^4 [1 - A\phi^{12}], \quad (A6)$$

$$M^4 [1 - A\phi^2], \quad (A7)$$

$$M^4 [1 - A\phi^4]. \quad (A8)$$

In all cases the mass scale and other parameters were chosen as in table IV to produce a $\delta\rho/\rho$ of roughly 2×10^{-5} .

APPENDIX B: MORE RESULTS

Table V gives more complete information on some of the results presented in subsection III C.

[1] E. Copeland, E. W. Kolb, A. R. Liddle, and J. E. Lidsey, Phys. Rev. D **48**, 2529 (1993).

[2] L. Knox, Phys. Rev. D **52**, 4307 (1995).

[3] A. Kosowsky and M. S. Turner, Phys. Rev. D **52**, 1739 (1995).

[4] G. Jungman, M. Kamionkowski, A. Kosowsky, and D. N. Spergel, Phys. Rev. D **54**, 1332 (1996).

[5] E. J. Copeland, I. J. Grivell, and A. R. Liddle, astro-ph/9712028.

[6] S. Dodelson, W. H. Kinney, and E. W. Kolb, Phys. Rev. D **56**, 3207 (1997).

[7] W. H. Kinney, A. Melchiorri, and A. Riotto, Phys. Rev. D **63**, 023505 (2001).

[8] S. Hannestad et al., astro-ph/0103047.

[9] S. H. Hansen and M. Kunz, hep-ph/0109252.

[10] M. Bucher, K. Moodley, and N. Turok (2000), astro-ph/0011025.

[11] A. H. Guth, Phys. Rev. D **23**, 347 (1981).

[12] A. Albrecht and P. Steinhardt, Phys. Rev. Lett. **48**, 1220 (1982).

[13] A. D. Linde, Phys. Lett. B **108**, 389 (1982).

[14] A. D. Linde, Phys. Lett. B **129**, 177 (1983).

[15] J. M. Bardeen, Phys. Rev. D **22**, 1882 (1980).

[16] S. Dodelson and E. Stewart, astro-ph/0109354.

[17] M. Tegmark and M. Zaldarriaga, Phys. Rev. D **66**, 103508 (2002).

[18] D. H. Lyth, hep-ph/9609431.

[19] A. R. Liddle and D. H. Lyth, *Cosmological Inflation and Large-Scale Structure* (Cambridge University Press, 2000).

[20] G. Dvali and S.-H. H. Tye, Phys. Lett. B **450**, 72 (1999).

[21] A. H. Guth and S.-Y. Pi, Physical Review Letters **49**, 1110 (1982).

[22] G. Shiu and S.-H. H. Tye, Phys. Lett. B **516**, 421 (2001).

[23] R. A. C. Croft et al., astro-ph/0012324.

[24] Y. Wang, D. N. Spergel, and M. A. Strauss, Astrophys. J. **20**, 510 (1999).

[25] M. Zaldarriaga and U. Seljak, Astrophys. J. **469**, 437 (1996).

[26] L. Knox, C. Skordis, and M. Kaplinghat, Astrophys. J. **578**, 665 (2002), astro-ph/0203413.

[27] J. A. Peacock and S. J. Dodds, Mon. Not. R. Astron. Soc. **267**, 1020 (1994).

[28] U. Seljak, Private communication (2002).

[29] As this work was completed we learned that the Sloan Digital Sky Survey is preparing to release a new Lyman- α dataset. While not as large as our survey which is “next generation” Lyman- α dataset simulated in this paper, it may have considerable importance to the issues raised in this article [28]

TABLE IV: Inflationary model parameters

Model #	M	A
1	10^{-3}	5×10^{-2}
2	10^{-3}	—
3	10^{-3}	—
4	10^{-4}	10^{-3}
5	$10^{-9/4}$	100
6	2×10^{-4}	5×10^{-3}
7	10^{-3}	10^{-2}
8	10^{-6}	$\frac{1}{4} \times 10^9$

TABLE V: Marginalized errors in all the power spectrum parameters for different experiments, using the weakest prior (I-6) from Table II.

Experiment	n_S	n_S'	$n_S^{(2)'} \backslash$	$n_S^{(3)'} \backslash$	$n_S^{(4)'} \backslash$	$n_S^{(5)'} \backslash$	$n_S^{(6)'} \backslash$
MAP-like w polarization	9.6×10^{-2}	2.6×10^{-1}	2.7×10^{-1}	3.9×10^{-2}	2.9×10^{-1}	4.3×10^{-1}	2.6×10^{-1}
	9.3×10^{-2}	2.3×10^{-1}	2.4×10^{-1}	3.5×10^{-2}	2.8×10^{-1}	4.2×10^{-1}	2.5×10^{-1}
PLANCK-like w polarization	3.5×10^{-2}	7.0×10^{-2}	8.4×10^{-2}	2.9×10^{-2}	1.8×10^{-1}	3.2×10^{-1}	2.0×10^{-1}
	2.0×10^{-2}	3.7×10^{-2}	5.2×10^{-2}	2.7×10^{-2}	1.8×10^{-1}	3.0×10^{-1}	1.9×10^{-1}
Next-Gen w polarization	9.5×10^{-3}	2.3×10^{-2}	1.8×10^{-2}	1.3×10^{-2}	5.0×10^{-2}	8.5×10^{-2}	5.3×10^{-2}
	5.2×10^{-3}	4.8×10^{-3}	1.0×10^{-2}	1.2×10^{-2}	4.7×10^{-2}	7.9×10^{-2}	4.9×10^{-2}
Super w polarization	7.1×10^{-3}	1.7×10^{-2}	1.5×10^{-2}	1.1×10^{-2}	4.1×10^{-2}	6.8×10^{-2}	4.0×10^{-2}
	2.8×10^{-3}	3.1×10^{-3}	5.6×10^{-3}	7.5×10^{-3}	2.2×10^{-2}	3.6×10^{-2}	2.2×10^{-2}